CCFE
CULHAM CENTRE FOR FUSION ENERGY

UK Atomic Energy Authority

UKAEA-CCFE-CP(23)62

D. Kumar, R. Clark, T. Martin, M. Zimina, P. Andresen, L. Volpe, R. Burrows

An Investigation into High Temperature Water Corrosion on Reduced-Activation Ferritic-Martensitic Steel Eurofer-97

An Investigation into High Temperature Water Corrosion on Reduced-Activation Ferritic-Martensitic Steel Eurofer-97

D. Kumar, R. Clark, T. Martin, M. Zimina, P. Andresen, L. Volpe, R. Burrows

This paper has been submitted to
21st International Conference on Environmental Degradation of Materials in Nuclear Power Systems - Water Reactors, St. John's, Newfoundland, Canada, 6-10 August 2023

An Investigation into High Temperature Water Corrosion on Reduced-Activation Ferritic-Martensitic Steel Eurofer-97

D. Kumar[1], R. Clark[1], T. Martin[2], M. Zimina[2], P. Andresen[3], L. Volpe[4], R. Burrows[1]

[1]National Nuclear Laboratory, Unit 102B, Stonehouse Park, Stonehouse GL10 3UT, UK
[2]Interface Analysis Centre, School of Physics, University of Bristol, HH Wills Physics Laboratory, Tyndall Avenue, Bristol, BS8 1TL, UK
[3]Lucideon Ltd, Queens Road, Penkhull, Stoke-on-Trent, Staffordshire, ST4 7LQ, UK
[4]United Kingdom Atomic Energy Authority, Culham Science Centre, Abingdon OX14 3DB

Abstract

The UK National Nuclear Laboratory (NNL) has been developing its capability in high-temperature water corrosion over the past years in collaboration with the University of Bristol, UK. Studies have been undertaken on nuclear fusion-specific material Eurofer-97, a reduced activation ferritic-martensitic steel. Eurofer-97 is a structural coolant-facing candidate material for the European DEMO water-cooled-lithium-lead breeder blanket design.

A microflow electrochemical cell assembly and Halbach array setup have been developed for use with the high-temperature water testing suite. The microflow cell assembly can provide in-situ electrochemical information on corrosion at increased flow velocities. The Halbach array allows experiments to be conducted to assess the impact of magnetic fields which are used for plasma confinement in DEMO. The effect of zinc addition is also investigated using the facility. For an insight into the effect of stress corrosion cracking, small-scale tensile specimens have been exposed to high-temperature (~300°C) water.

NNL, in collaboration with the UK Atomic Energy Authority (UKAEA) and Lucideon Ltd, are to study the high-temperature water oxidation and environmentally-assisted cracking behaviour of Eurofer-97 as part of the EUROfusion programme. Presented are different experimental setups used to explore the aqueous corrosion of Eurofer-97 as well as preliminary information on the upcoming programme with UKAEA.

1. Introduction

The safe operation of nuclear fusion power plants, including the European demonstrational power station (DEMO), are reliant on research of suitable structural materials for the challenging environments within the reactor. The coolant circuit is an example of these harsh conditions, where the chosen structural materials will be exposed to high energy neutron fluxes, thermal transients from plasma-first wall contact, high magnetic fields, and corrosion from the chosen coolant [1–4]. Proposed materials for the water-cooled lithium-lead (WCLL) breeder blanket will have to be studied for their aqueous corrosion behaviour under fusion reactor conditions. It is important to fully characterise corrosion behaviours to mitigate possible coolant circuit material failure, and doing so prevent high-temperature, high-pressure, (HTHP) water leaks as well as coolant-tritium breeding material contact in the blanket module between water and eutectic lithium-lead.

Eurofer-97 is Europe's candidate structural material for the WCLL breeder blanket. Eurofer-97 is a reduced-activation ferritic-martensitic (RAFM) steel [1], [2]. RAFM steels have been chosen as suitable structural materials for the EUROfusion DEMO reactor as ferritic-martensitic steels have been found to perform favourably under irradiation, exhibiting resistance to radiation swelling and a small (-50 to 0°C) increase in ductile to brittle transition temperature [5], [6]. These steels are classed as reduced-activation due to the substitution of elements such as Mo, Nb, and Ni which can be transmuted into long-lived radionuclides under neutron irradiation for W, V, and Ta, resulting in less challenging radioactive waste upon decommissioning [7]–[9]. Within these RAFM steels, the dominant secondary phases are $M_{23}C_6$ carbides and MX precipitates, where M is a metal and X is carbon or Nitrogen [10]–[12]. Various RAFM steels have been developed by different countries, such as F82H for Japan, with Eurofer-97 having the composition Fe–9Cr–1W–0.2V–0.12Ta to be used in DEMO [13]–[18].

In order to study the aqueous corrosion of Eurofer-97 in simulated fusion reactor cooling circuit environments the UK National Nuclear Laboratory (NNL) in collaboration with the University of Bristol (UoB) have been developing an autoclave facility. With this, samples of coolant circuit material can be exposed to HTHP water while controlling the water chemistry and administering different chemical additives and fusion specific factors such as magnetic fields. The WCLL coolant will share similarities to fission light water reactor circuits. Therefore it is thought that corrosion mitigation techniques learned from fission reactors may be able to be applied to the WCLL coolant. These include the addition of hydrogen to combat the increased generation of oxidising radiolysis products from the 14 MeV neutron flux through the coolant water [19], [20]. Noble metal chemical addition (NMCA) could also be investigated as it has been shown that the formation of noble metal nanoparticles on the material surface catalyses the recombination reaction minimising the amount of hydrogen addition required [21]. The addition of zinc to the coolant may also be used as a corrosion mitigation strategy; as it forms a more dense and stable oxide layer and may prevent the uptake of ^{60}Co into the oxide layer, thereby lowering radiation fields [22]–[24]. Results from zinc addition on Eurofer-97 oxidation are presented in this paper along with other experiments demonstrating the capabilities of the autoclave facility.

2. Experimental procedures

For autoclave exposures Eurofer-97 specimens were ground to a 15.3 µm finish on each face using progressively finer SiC paper. Specimens are cleaned with water and detergent between polishing steps and ultrasonically cleaned with acetone, ethanol, isopropanol, and demineralised water prior to corrosion testing. Eurofer-97 samples are cut into ~5 x 5 x 1 mm coupons for corrosion testing. For the microchannel assembly a larger 50 x 5 x 2 mm sample was required and 15.5 x 1.6 x 1.6 mm matchstick samples were used for magnetic field experiments as samples are held within $1/8^{th}$ inch (3.175 mm) diameter Swagelok tubing, as opposed to the main vessel.

Eurofer-97 specimens are analysed after corrosion experiments using a FEI Helios 600 dual beam (DB) with combined scanning electron microscope (SEM) and focused ion beam (FIB) sources with Oxford Instruments energy dispersive X-rays (EDX) and scanning transmission electron microscopy (STEM) capabilities. This was used to image surface topography,

perform FIB milling for cross sections and lamella sample preparation, and STEM imaging. Transmission electron microscopy (TEM) was performed using a JEOL 2100F TEM.

3. High-temperature corrosion of Eurofer-97 / Development of autoclave facility capabilities

WCLL breeder blankets will nominally use 15.5 MPa water at 295 – 328 °C with a slightly alkaline (7-8) $pH_{300\ °C}$ [25], [26]. An autoclave facility has been developed using a 500 ml stainless steel Baskerville autoclave, modified with a HTHP flow loop using Swagelok piping and fixtures allowing the replication of specific WCLL conditions.

Autoclave temperatures are monitored via thermocouples placed throughout the flow circuit as well pressure, using Omega PXM319-350GI pressure transducers. Dissolved oxygen is measured using a 3600 series analyser from Orbisphere Laboratories and conductivity via a Swan Analytical Instruments FAM RESCON U Conductivity probe. A Cole-Palmer MasterFlex High-Flow Dual Piston Pump is used for controlling the water flow rate. Future development of this loop is expected to include an electrochemical hydrogen generator apparatus and dissolved hydrogen monitoring instrumentation.

As a baseline, Eurofer-97 samples have been exposed to deaerated water at high temperatures and pressures. This was conducted to understand the oxidation behaviour of this material in coolant conditions prior to adding any other factors such as a magnetic field or altering the water chemistry. Figure 1 shows the oxide layer that forms on Eurofer-97 after exposure to ultra pure water at 331 ± 0.4 °C and 13.5 ± 0.1 MPa for 100 h at a flow rate of 10 ml/min.

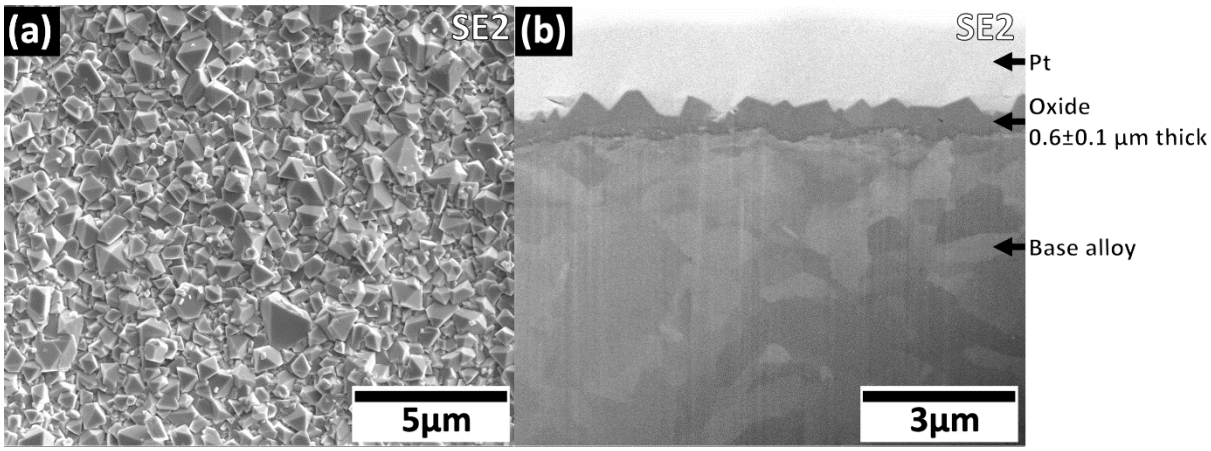

Figure 1: Secondary electron SEM micrographs of Eurofer-97 samples exposed to 331 ± 0.4 °C ultra pure water at 13.5 ± 0.1 MPa for 100 h. (a) surface oxide morphology, (b) FIB-milled cross section through Pt and oxide layer into the bulk material.

SEM showed that the surface of the material was covered in faceted octahedral shaped oxide crystals. FIB milling was used to obtain a cross section through the oxide layer. A Pt layer was deposited on top of the area of interest to project it during FIB milling. The oxide crystals were of the order ~100 nm in diameter imaged from above (Figure 1.a). The oxide layer was measured to be 0.6 ± 0.1 µm thick from the cross section (Figure 1.b).

4. Zinc addition

The effects of zinc addition in WCLL coolant circuits has not been widely investigated [2]. The formation of a more dense and stable oxide that prevents the uptake of radioactive ^{60}Co containing oxide into the surface layers would be beneficial for fusion application as it is in fission light water reactors (LWRs) where zinc addition is currently employed [22], [24], [27], [28]. For type 304 and 316 stainless steels the addition of zinc to the coolant water has been more thoroughly researched and it has been observed that $ZnCr_2O_4$ forms with a more compact lattice parameter than $FeCr_2O_4$ that forms in its absence [28], [29].

To investigate the effects of zinc addition on the oxidation of Eurofer-97 in simulated reactor conditions a second autoclave flow loop was fabricated and commissioned, with the same design as the primary flow circuit using flow rate of 10 ml/min. Zinc was introduced into the feed reservoir using zinc acetylacetonate in a syringe pump to achieve ~100 ppb zinc. The experiment was performed at 330 ± 2 °C for 100 h pressurised to 13.0 ± 0.9 MPa.

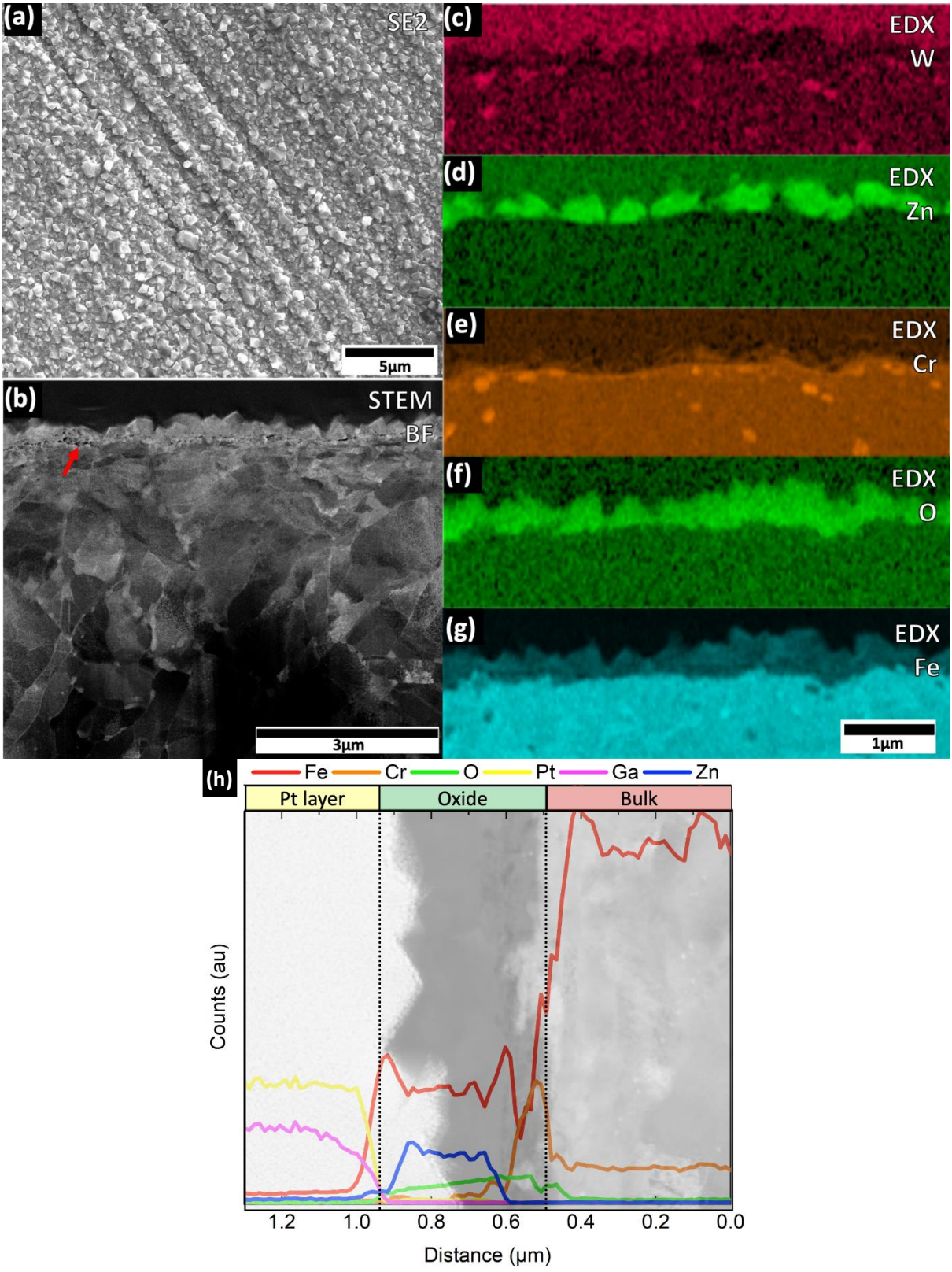

Figure 2: Eurofer-97 specimen exposed to ~100 ppb zinc at 330 ± 2 °C for 100 h at 13.0±0.9 MPa. (a) Secondary electron image of surface morphology, (b) STEM bright field (BF) image of lamella sample showing cross section through oxide layer with red arrow indicating region of porosity, (c-g) STEM EDX maps showing W, Zn, Cr, O, and Fe concentrations, (h) showing STEM EDX line scan through oxide layer.

Figure 2.a shows a similar covering of oxide crystals to that seen in Figure 1.a, comparing the surface morphologies of the oxide layers formed with and without zinc addition. Upon cross sectioning and subsequent lamella sample fabrication for STEM imaging it can be seen that the oxide layer is noticeably thinner on the sample dosed with zinc at 0.3 ± 0.1 µm thick. This is consistent with other work such as for zinc addition on type 316 [24]. The STEM bright field image in Figure 2.b shows the surface oxide atop the bulk steel separated by a small region of porosity (red arrow). The dark area at the top of the image is the deposited Pt layer. STEM EDX maps confirm that zinc has been incorporated into the oxide layer formed on Eurofer-97, Figure 2.d.

5. Microchannel assembly

A microchannel assembly was designed and fabricated by NNL and UoB in order to contain a sample that forms part of the channel within. The channel is 25 mm long with a cross section of 1 × 1 mm^2. Samples for assembly are ~50 × 5 × 2 mm^3 sections of Eurofer-97 sitting upon gaskets initially made from polytetrafluoroethylene (PTFE) (for pressure testing, and ambient temperature experiments) and produced from polyetheretherketone (PEEK) for high temperature usage.

This assembly is designed to be fitted to the autoclave outlet so that HTHP water can flow across the sample. A bespoke electrochemical gasket stack allows corrosion monitoring of samples within the microchannel assembly in-situ via electrochemical techniques. Under HTHP conditions this gasket stack has been used to conduct electrochemical impedance spectroscopy (EIS) of a Eurofer-97 sample exposed to ultra-pure water (18.2 MΩ·cm) up to 200 °C at 3 MPa.

A proof-of-concept experiment was performed in which the conditions within the autoclave changed through three different regimes over 34 h. Initially the Eurofer-97 specimen was exposed to 150 °C for 6 h before increasing the temperature to 200 °C for 28 h. After 21 h, potassium hydroxide (KOH) was added to the feed water as a chemistry change to increase the *pH*. KOH was investigated as a substitute for lithium hydroxide (LiOH) which is proposed for use in WCLL coolant to achieve the desired moderately alkaline solution [2]. These regimes are reflected in the datalogger readout for the temperature at points around the flow circuit in Figure 3.

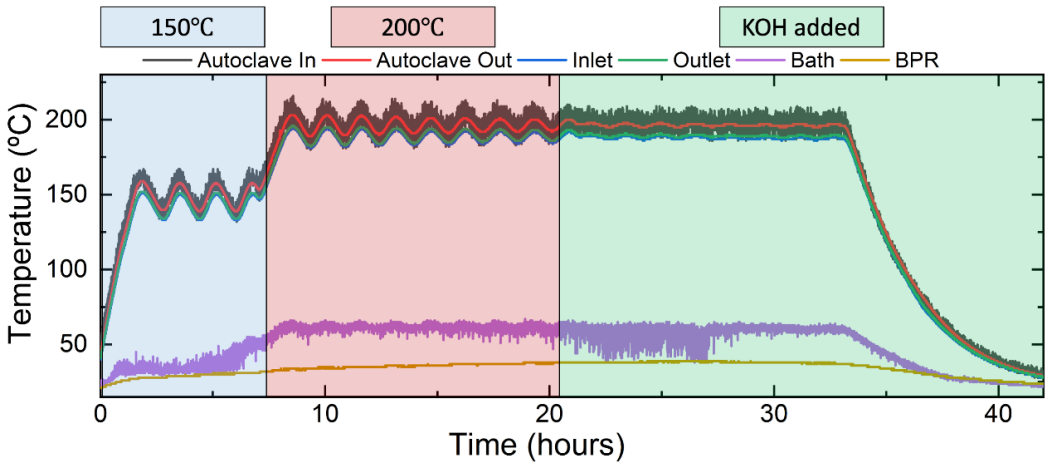

Figure 3: Temperature data from thermocouples around the flow circuit for the microchannel assembly experiment.

EIS was performed using a Gamry Interface 1000 potentiostat from 100 kHz to 100 mHz with a 10 mV excitation from the open circuit potential (OCP). ZView 4 (Scribner Associates Inc.) was used to fit the EIS data to the equivalent circuit chosen to represent the system in Figure 4. This circuit with two RC time constants was chosen, with the first RC pair representing the surface oxide layer with resistance and capacitance R_o and C_o for the high frequency data. The second RC pair represents the charge transfer resistance, R_{ct}, and the double layer capacitance represented by a constant phase element CPE_{dl} for the lower frequency data. R_s is the solution resistance.

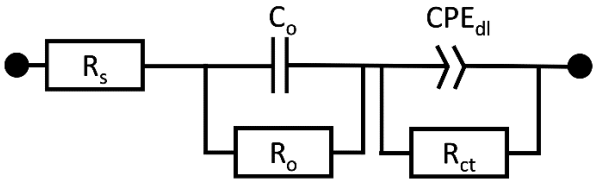

Figure 4: Equivalent circuit used to fit EIS data from microchannel assembly experiment.

The values obtained from this fit for the EIS data collected during the experiment are shown in Figure 5. The error bars are obtained from the error of the ZView 4 fit for each data set. The data obtained from EIS appears to follow the changes made to the temperature and water chemistry. Three distinct steps can be seen in the surface oxide resistance and capacitance data as the conditions change. R_o decreases as the temperature increases, and again decreases as KOH is added. C_o increases with temperature and slightly decreases when KOH is added. The charge transfer resistance and the double layer capacitance respond to the temperature change and apparently less so to the chemistry change. It is important to note that the value for solution resistance is given as a negative number from the equivalent circuit fitting. This is clearly not physical and is requires further experiments to be performed with this electrochemical setup to investigate this phenomenon. This has been seen in the literature for materials undergoing active to passive transitions [30], [31]. The setup uses a three electrode system in which stainless steel foils are used for the counter and reference electrodes and as a contact for the Eurofer-97 working electrode. Therefore it is a pseudo-electrode and could lead to these errors seen in the data. In the future Pt could be used as an alternative pseudo-reference electrode.

Nevertheless, the EIS data from preliminary in-situ experiments measuring Eurofer-97 corrosion are successful in that changes in conditions over a short timeframe are indeed reflected in the data. Going forward, this assembly with electrochemical measurement can be used in further experiments to investigate differing water chemistries as well as the effects of applying a magnetic field and changing its orientation relative to the sample.

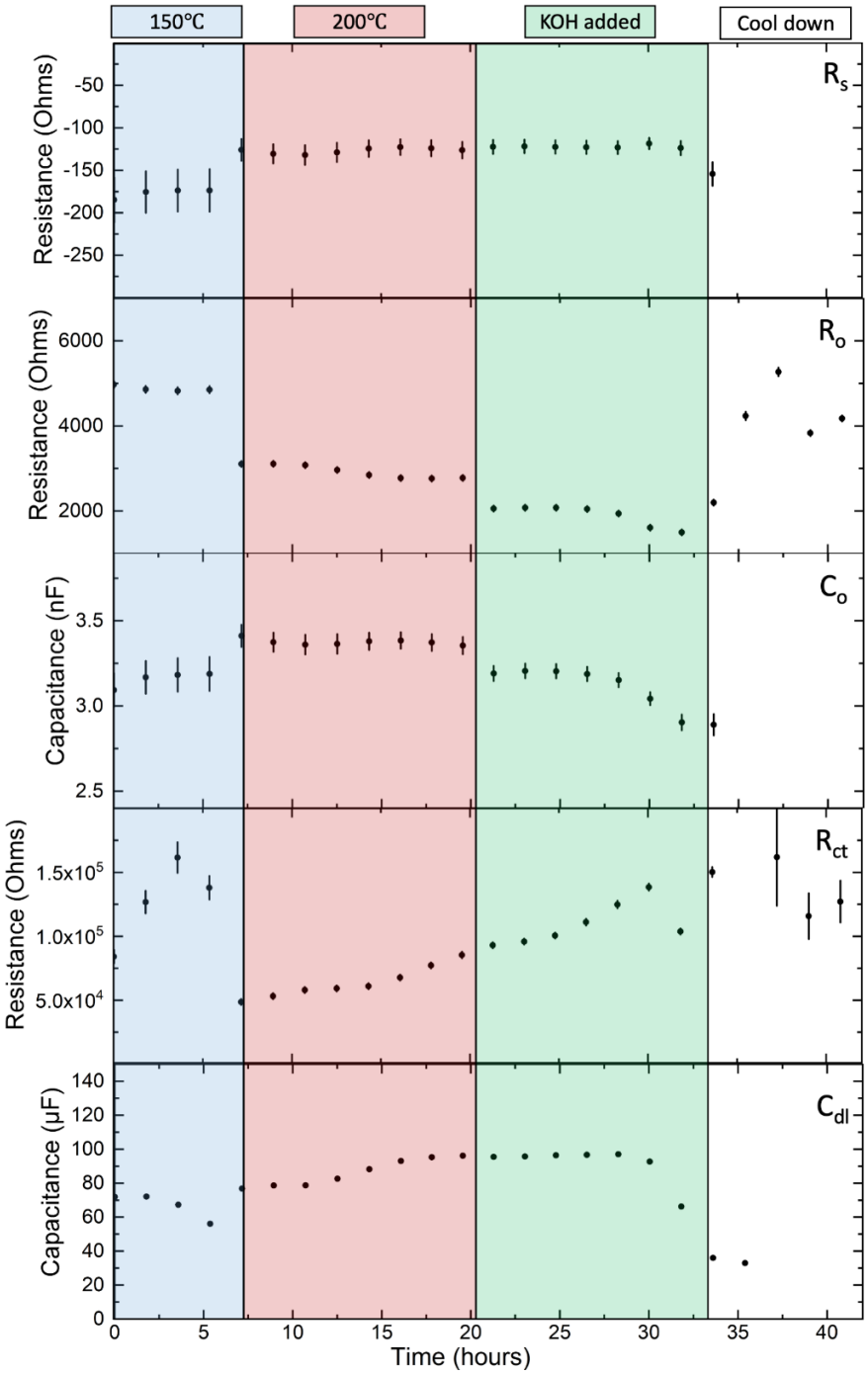

Figure 5: EIS values obtained through fitting data to equivalent circuit in Figure 4. R_s – solution resistance. R_o, C_o – resistance and capacitance of surface oxide. R_{ct} – charge transfer resistance. CPE_{dl} – constant phase elements used to fit double layer capacitance

6. Magnetic field effects

Over the breeder blanket modules of a fusion reactor a high magnetic field is expected to be present with a strength of 9.9 T to 8.6 T, and 4.4 T to 3.7 T over the inboard and outboard blanket components respectively [4]. Magnetic fields have been observed to effect aqueous corrosion in other systems outside of fusion applications through magnetohydrodynamic (MHD) effects [32], [33]. It is proposed that the orientation of the magnetic field to the surface of the corroding material can either enhance or suppress corrosion processes through

interactions with corrosion products. If the magnetic field is parallel to the sample surface local Lorentz stirring may increase mass transport of ions in solution.

With such a high magnetic field present over the WCLL blanket modules it is sensible to investigate the aqueous corrosion of Eufoer-97 in the presence of a magnetic field. This is in order to determine whether this is a factor that warrants further investigation and consideration as these effects are not currently well understood. Eurofer-97 is also expected to form magnetite in WCLL conditions, Fe_3O_4 has a high magnetic moment and could be affected by the magnetic field.

To investigate this the autoclave facility can be modified so that the sections of piping connected to the autoclave outlet are exchanged for sections designed to house three samples. One upstream sample, one downstream sample, and a sample in the middle within a section of piping located inside the annulus of a Halbach array. This array generates a uniform 0.88 T magnetic field within its annulus. An upstream and downstream control sample are used to account for any effect from the temperature drop the further the sample is from the autoclave outlet. The upstream, in-field, and downstream sample reached temperatures of 304 °C, 293 °C, and 280 °C respectively at 12.4 MPa for 500 h at a flowrate of 10 ml/min.

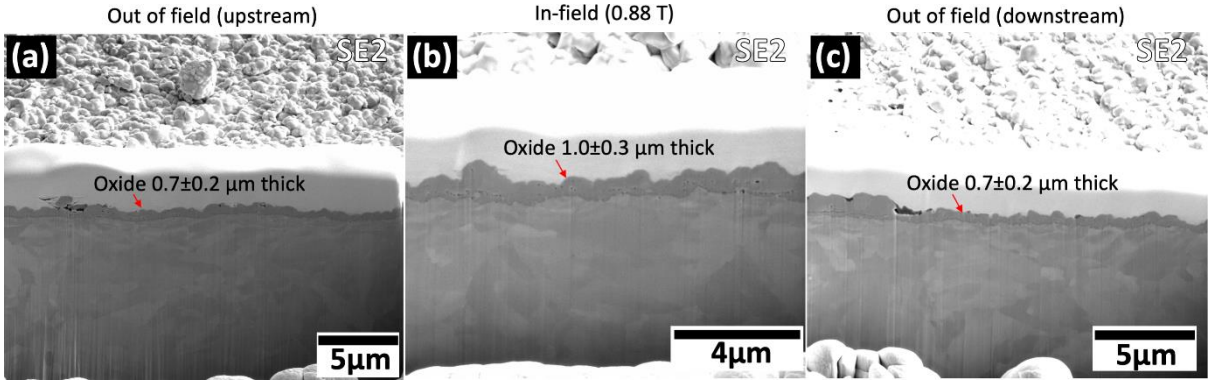

Figure 6: Secondary electron SEM micrographs of FIB-milled cross section of Eurofer-97 samples exposed to 12.4 MPa ultrapure water for 500 h at (a) 304 °C out of field upstream sample, (b) 293 °C in-field sample, (c) 280 °C out of field downstream.

Figure 6 shows FIB-milled cross sections through the protective Pt layer, the surface oxide layer, and into the bulk alloy for all three samples used in the magnetic corrosion experiment. All samples were covered in a layer of rounded oxide crystals of the same order of magnitude in diameter. The rounded oxide crystals versus more faceted crystals seen in Figures 1 and 2 could be due to the 10 ml/min flow over these matchstick samples held within tubing instead of being placed within the autoclave vessel. The duration of the test in this section is also 500 h versus 100 h in previous sections, which may also have an effect. FIB-milled cross sections were used to investigate any difference in thickness between the out of field and the in-field sample oxide layers. The thicknesses were measured to be 0.7 ± 0.2 µm, 1.0 ± 0.3 µm, and 0.7 ± 0.2 µm for the upstream, in-field, and downstream samples indicating no discernible difference, with error, between the samples.

For this experiment matchstick samples of Eurofer-97 are placed within the tubing so they experience a significant flow increase compared to when samples are placed within the autoclave vessel. The flow over the samples may be negating any effects the presence of the magnetic field has on the mass transport in the system. Therefore all samples display the

same corrosion behaviour and oxide appearance as one another. An interesting extension of this work could look at using the electrochemical setup to probe more subtle changes in corrosion rate for a sample inside and outside of a magnetic field as well as with changing orientation. This could be performed at lower or no flow rate as well to assess flow rate as a factor.

7. Environmentally assisted cracking

A strain rig was designed in order to investigate environmentally assisted cracking (EAC) of specimens within the autoclave. EAC could occur in Eurofer-97 components if they are found in a specific environment to induce EAC under residual or applied stresses [34]. This rig enabled samples to be exposed to autoclave experiment conditions whilst a reproducible strain is applied. Figure 7 shows an image of the strain rig and a Eurofer-97 specimen. A torque applied through the top screw of the rig which applies a uniaxial stress to the sample within.

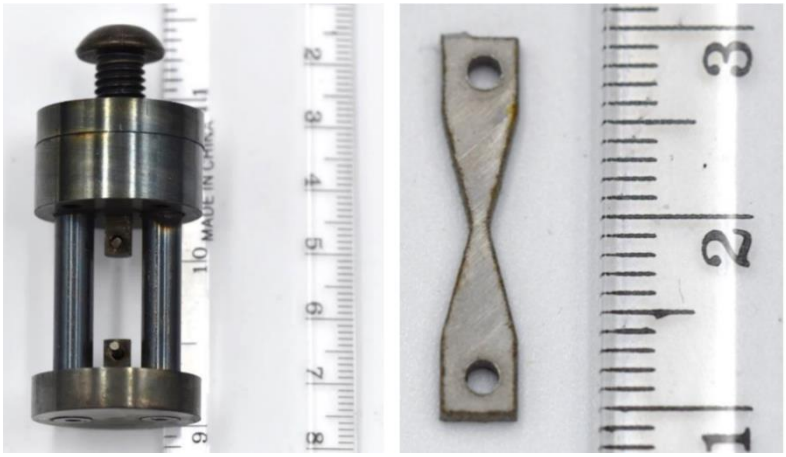

Figure 7: Images of a stress rig and Eurofer-97 waist-section sample (pre-surface preparation)

Using three strain rigs, Eurofer-97 was investigated in comparison to type 316 and thermally sensitised 304 stainless steels in the same autoclave EAC experiment. Thermally sensitised (60 h at 600 °C) 304 stainless steel is expected to undergo stress corrosion cracking (SCC) due to the sensitisation and provides comparison against the two other specimens. The strain rigs were torqued to 1.5 ± 0.5 Nm with a torque wrench which was found to be sufficient to hold the specimens at yield stress and cause cold work in the waisted region. The mechanical properties of each sample will differ so there are improvements that can be made to this procedure for each specimen's specific yield stress. The autoclave exposure was a once-through experiment with a low flow rate of 0.3 ml/min at 300 °C and 15 MPa for 100 h.

SEM imaging of the samples post-exposure showed faceted oxide crystals across all three specimens, likely magnetite, Figure 8. Eurofer-97 and 316 samples showed no indication of any cracking after the exposure but the 304 sample experienced crack initiation in the waist section of the specimen. SEM imaging found this to be intergranular cracking as it followed grain boundaries. It is expected that sample failure would have occurred had the experiment ran for longer. This short test using the strain rig showed that Eurofer-97 and type 316 stainless steel showed no signs of SCC for this exposure when compared to sensitised type

304 stainless steel. In the future, further tests can be performed using this small-scale stress rig in order to explore EAC behaviour of Eurofer-97 specimens in different conditions relevant to WCLL coolant systems. A stress is expected on the structural materials due to the magnetic field in the system which should then be investigated in terms of potential SCC initiation [35].

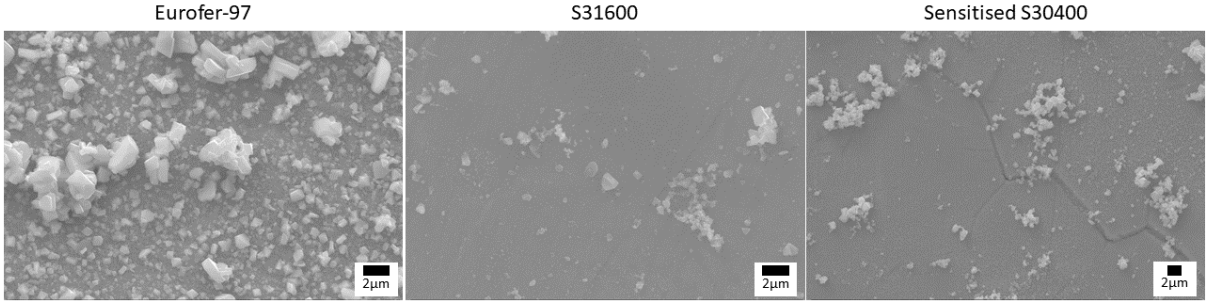

Figure 8: Secondary electron micrographs of Eurofer-97, 316316, and thermally sensitised 304304 after 300 °C, 15 MPa autoclave exposure for 100 h.

8. Radiolysis modelling

Within the WCLL coolant circuit the coolant itself will be under high neutron and gamma radiation leading to radiolytic decomposition resulting in the production of oxidising species such H_2O_2 and O_2. These species can lead to an increase in OCP / electrochemical corrosion potential (ECP) within the coolant water which could result in increased corrosion of Eurofer-97 tube components. Higher ECP can also increase cracking susceptibility for material under stress in reactor cooling systems. Modelling has been conducted to establish the radiolytic species and respective concentrations at different locations of the reactor circuit.

9. Ion-irradiation

The structural materials inside nuclear fusion reactor breeder blankets will be bombarded by high energy 14 MeV neutrons. This irradiation can cause damage to materials through displacement of atoms leading to the formation of vacancies, interstitials, line defects, and voids within the crystal lattice as well as altering precipitation formation. These microstructural changes can affect the material's overall mechanical properties. When evaluating the corrosion behaviour of Eurofer-97 in WCLL coolant circuit conditions it is therefore important to consider these radiation-induced structural changes in terms of their knock-on effect on corrosion/cracking susceptibility.

To investigate irradiation effects on corrosion behaviour, Eurofer-97 was self-ion irradiated using Fe ions with a peak fluence of 0.69×10^{17} cm^{-2} at the beam centre. This was conducted isothermally at 340 °C at 89.73 MeV under vacuum. Stopping range of ions in matter (SRIM) calculations predicated a damage depth of 7.2 µm. Irradiated Eurofer-97 was then exposed to 300 °C ultra pure water at 13 MPa for 240 h using the autoclave facility. A flow rate of 10 ml/min was set to refresh the solution.

Analysis of samples post-corrosion was performed through the fabrication of TEM lamella samples using a FIBSEM microscope, Figure 9, these results have been prepared in the form of a journal paper which is currently undergoing peer review.

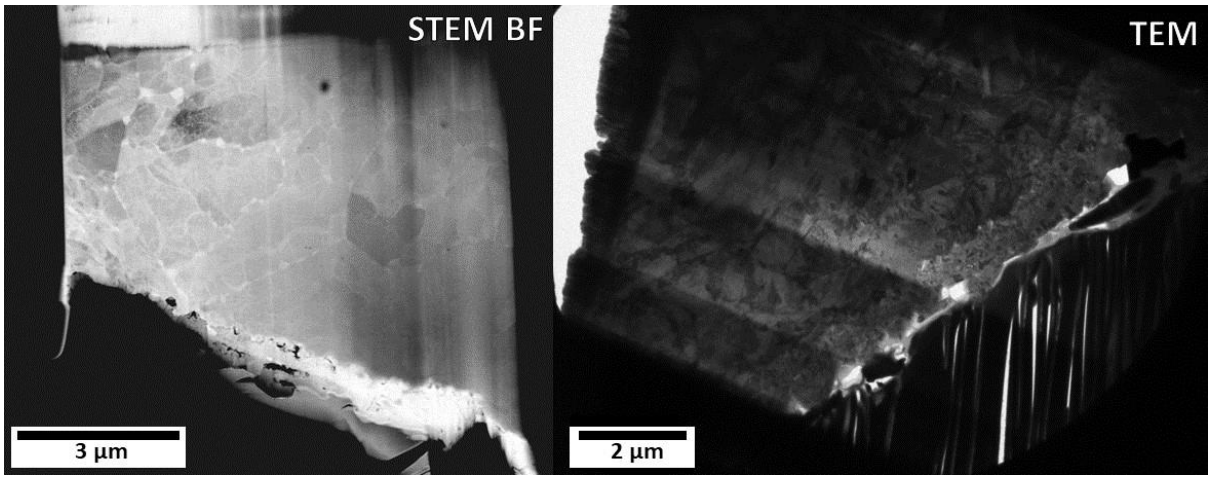

Figure 9: (a) STEM bright field (BF) and (b) TEM micrographs of ion-irradiated Eurofer-97 lamella specimen

10. Upcoming work

As part of EUROfusion, a three-year programme studying high-temperature aqueous corrosion of Eurofer-97 will soon be underway as a collaboration between NNL with the UK Atomic Energy Authority (UKAEA) and Lucideon Ltd. This work will further explore the oxidation and EAC behaviour of Eurofer-97 when exposed to HTHP water conditions relevant to the DEMO concept design. This project will aim to perform oxidation experiments with carefully controlled and monitored conditions in order to gauge the effects of different pH levels and Zn injections. Experiments will be performed in between *pH* equal to 7 – 8.4 using KOH as *pH* moderator. Further experiments may then be performed using LiOH and results compared to establish if there are any differences due to the different cations. Autoclave experiments will use a recirculating loop by carefully controlling the water chemistry for a minimum of 500 h.

EAC behaviour will also be investigated through the fabrication and testing of compact tension (CT) specimens. Crack growth rate will be able to be monitored in response to applied changes to autoclave condition during sample exposure (*e.g.*, changing the *pH*). There is also scope to further investigate magnetic field effects on aqueous corrosion behaviour to expand on the initial experiments discussed in section 5. This collaborative project also aims to further modelling work looking into calculating the ECP for DEMO breeder blanket cooling circuits as well as looking at the impact of the coolant on divertor material CuCrZr. This will look at concentrations of radiolysis products in order to determine the required hydrogen concentration required in order to suppress them.

11. Conclusion

This paper has showed the different capabilities of the autoclave facility developed in collaboration between NNL and the University of Bristol. This facility has been used to begin investigating the aqueous corrosion of Eurofer-97 for the WCLL breeder blanket design. Research into oxidation and cracking behaviour of Eurofer-97 is critical to the safe operation

of nuclear fusion power plants. The autoclave facility has been used to successfully expose Eurofer-97 specimens to ultra pure water under HTHP conditions, as well as a variety of water chemistries including zinc and KOH additions. A bespoke microchannel assembly was used with an electrochemical gasket stack to perform EIS in-situ. Magnetic field effects were investigated through the modification of the flow loop to accommodate a Halbach array magnet. An EAC experiment was performed comparing Eurofer-97 to sensitised type 304 and 316 stainless steels using a uniaxial strain rig. Radiolysis modelling has also been performed in an attempt to assess the levels of oxidising species expected within the water coolant.

Further work in collaboration with UKAEA and Lucideon Ltd aims to continue investigations into Eurofer-97 oxidation and EAC behaviour in controlled and monitored conditions. CT specimens will be used in order to measure crack growth rates in response to changing autoclave conditions such as pH.

Acknowledgements

The authors would like to acknowledge Dr Chris Harrington[1] for supplying the Eurofer97 sample material. Chris Jones[2] is acknowledged for this support in using the FIB-SEM instrument for the several TEM specimens prepared with the *in situ* lift out technique. Support from the UK National Nuclear Laboratory internal research and development Core Science Programme is acknowledged. The work was performed using the University of Bristol Interface Analysis Centre equipment. Funding provided through EPSRC and NNL funded doctoral training partnership PhD project.

Transmission electron microscopy studies carried out in the Chemical Imaging Facility at the University of Bristol by Jean-Charles Eloi[3], with equipment funded by EPSRC under Grant "Atoms to Applications" Grant ref. EP/K035746/1.

This work has been carried out within the framework of the EUROfusion Consortium and has received funding from the Euratom research and training programme 2014–2018 under grant agreement No 633053. The views and opinions expressed herein do not necessarily reflect those of the European Commission.

12. References

[1] R. Aymar, P. Barabaschi, and Y. Shimomura, “The ITER design,” *Plasma Phys. Control. Fusion*, vol. 44, no. 5, pp. 519–565, 2002, doi: 10.1088/0741-3335/44/5/304.

[2] C. Harrington *et al.*, “Chemistry and corrosion research and development for the water cooling circuits of European DEMO,” *Fusion Eng. Des.*, vol. 146, pp. 478–481, Sep. 2019, doi: 10.1016/j.fusengdes.2018.12.095.

[3] D. Kumar *et al.*, “The effects of fusion reactor thermal transients on the microstructure of Eurofer-97 steel,” *J. Nucl. Mater.*, vol. 554, p. 153084, 2021, doi: 10.1016/j.jnucmat.2021.153084.

[1] UK Atomic Energy Authority, Culham Centre for Fusion Energy, Abingdon, Oxon, OX143DB, UK

[2] Interface Analysis Centre, School of Physics, University of Bristol, HH Wills Physics Laboratory, Tyndall Avenue, Bristol, BS8 1TL, UK

[3] School of Chemistry, University of Bristol, Cantock’s Close, Bristol, BS8 1TS, UK

[4] R. Burrows *et al.*, “The possible effect of high magnetic fields on the aqueous corrosion behaviour of Eurofer,” *Fusion Eng. Des.*, vol. 136, pp. 1000–1006, Nov. 2018, doi: 10.1016/j.fusengdes.2018.04.054.
[5] O. Ostrovski and D. K. Belashchenko, “Thermophysical properties and structure of liquid Fe-C alloys,” *High Temp. - High Press.*, vol. 42, no. 2, pp. 137–149, 2013.
[6] K. Shiba and A. Hishinuma, “Low-temperature irradiation effects on tensile and Charpy properties of low-activation ferritic steels,” *J. Nucl. Mater.*, vol. 283–287, no. PART I, pp. 474–477, Dec. 2000, doi: 10.1016/S0022-3115(00)00369-X.
[7] Z. Tong and Y. Dai, “The microstructure and tensile properties of ferritic/martensitic steels T91, Eurofer-97 and F82H irradiated up to 20dpa in STIP-III,” *J. Nucl. Mater.*, vol. 398, no. 1–3, pp. 43–48, Mar. 2010, doi: 10.1016/j.jnucmat.2009.10.008.
[8] D. R. Harries, G. J. Butterworth, A. Hishinuma, and F. W. Wiffen, “Evaluation of reduced-activation options for fusion materials development,” *J. Nucl. Mater.*, vol. 191–194, pp. 92–99, Sep. 1992, doi: 10.1016/S0022-3115(09)80015-9.
[9] A. Kohyama, A. Hishinuma, D. S. Gelles, R. L. Klueh, W. Dietz, and K. Ehrlich, “Low-activation ferritic and martensitic steels for fusion application,” *J. Nucl. Mater.*, vol. 233–237, no. PART 1, pp. 138–147, 1996, doi: 10.1016/S0022-3115(96)00327-3.
[10] R. C. Thomson and H. K. D. H. Bhadeshia, “Carbide precipitation in 12Cr1MoV power plant steel,” *Metall. Trans. A*, vol. 23, no. 4, pp. 1171–1179, Apr. 1992, doi: 10.1007/BF02665048.
[11] F. Abe, H. Araki, and T. Noda, “Effect of microstructural evolution in bainite, martensite, and δ ferrite on toughness of Cr–2W steels,” *Mater. Sci. Technol.*, vol. 8, no. 9, pp. 763–773, Sep. 1992, doi: 10.1179/mst.1992.8.9.763.
[12] W. B. Jones, C. R. Hills, and D. H. Polonis, “Microstructural evolution of modified 9Cr-1Mo steel,” *Metall. Trans. A*, vol. 22, no. 5, pp. 1049–1058, May 1991, doi: 10.1007/BF02661098.
[13] R. Holmes, B. Li, L. Cui, S. Kano, H. Yang, and H. Abe, “Preliminary investigation of Cr-coated F82H: Evolution of microstructure and mechanical properties at the F82H/Cr interface during solid-state diffusion bonding above Ac1 temperature,” *J. Nucl. Mater.*, vol. 578, p. 154371, May 2023, doi: 10.1016/j.jnucmat.2023.154371.
[14] F. Romanelli *et al.*, “Fusion Electricity A roadmap to the realisation of fusion energy,” *EFDA*, 2012.
[15] J. Aubert, G. Aiello, N. Jonquères, A. Li Puma, A. Morin, and G. Rampal, “Development of the water cooled lithium lead blanket for DEMO,” *Fusion Eng. Des.*, vol. 89, pp. 1386–1391, Oct. 2014, doi: 10.1016/j.fusengdes.2014.01.061.
[16] R. Lindau *et al.*, “Present development status of EUROFER and ODS-EUROFER for application in blanket concepts,” *Fusion Eng. Des.*, vol. 75–79, pp. 989–996, Nov. 2005, doi: 10.1016/J.FUSENGDES.2005.06.186.
[17] Y. Poitevin *et al.*, “Progresses and challenges in supporting activities toward a license to operate European TBM systems in ITER,” *Fusion Eng. Des.*, vol. 89, no. 7–8, pp. 1113–1118, Oct. 2014, doi: 10.1016/J.FUSENGDES.2014.03.071.
[18] H. Tanigawa *et al.*, “Development of benchmark reduced activation ferritic/martensitic steels for fusion energy applications,” *Nucl. Fusion*, vol. 57, no. 9, 2017, doi: 10.1088/1741-4326/57/9/092004.
[19] E. Ibe, M. Nagase, M. Sakagami, and S. Uchida, “Radiolytic environments in boiling water reactor cores,” *J. Nucl. Sci. Technol.*, vol. 24, no. 3, pp. 220–226, Mar. 1987, doi: 10.1080/18811248.1987.9735796.
[20] Y. Wada, S. Uchida, M. Nakamura, and K. Akamine, “Empirical understanding of the dependency of hydrogen water chemistry effectiveness on BWR designs,” *J. Nucl. Sci. Technol.*, vol. 36, no. 2, pp. 169–178, 1999, doi: 10.1080/18811248.1999.9726195.

[21] P. V. Grundler and S. Ritter, “Noble Metal Chemical Addition for Mitigation of Stress Corrosion Cracking: Theoretical Insights and Applications,” *Powerpl. Chem.*, vol. 16, no. 2, pp. 76–93, 2014.
[22] T. Ohashi, T. Ito, H. Hosokawa, M. Nagase, and M. Aizawa, “Investigation of cobalt buildup behavior and suppression by zinc injection on stainless steel under HWC conditions using simultaneous continuous measurements of corrosion and cobalt buildup,” *J. Nucl. Sci. Technol.*, vol. 52, no. 4, pp. 588–595, 2015, doi: 10.1080/00223131.2014.967323.
[23] T. Terachi, K. Fujii, and K. Arioka, “Microstructural characterization of scc crack tip and oxide film for SUS 316 stainless steel in simulated PWR primary water at 320°C,” *J. Nucl. Sci. Technol.*, vol. 42, no. 2, pp. 225–232, 2005, doi: 10.1080/18811248.2005.9726383.
[24] S. Holdsworth *et al.*, “The effect of high-temperature water chemistry and dissolved zinc on the cobalt incorporation on type 316 stainless steel oxide,” *Corros. Sci.*, vol. 140, no. June 2017, pp. 241–251, Aug. 2018, doi: 10.1016/j.corsci.2018.05.041.
[25] L. V. Boccaccini *et al.*, “Objectives and status of EUROfusion DEMO blanket studies,” *Fusion Eng. Des.*, vol. 109–111, pp. 1199–1206, Nov. 2016, doi: https://doi.org/10.1016/j.fusengdes.2015.12.054.
[26] D. D. Meis, E. L. Piccolo, and R. Torella, “Corrosion resistance of RAFM steels in pressurized water for nuclear fusion applications,” no. April, p. 14, 2017.
[27] X. Liu, X. Wu, and E.-H. Han, “Influence of Zn injection on characteristics of oxide film on 304 stainless steel in borated and lithiated high temperature water,” *Corros. Sci.*, vol. 53, no. 10, pp. 3337–3345, Oct. 2011, doi: 10.1016/j.corsci.2011.06.011.
[28] S. E. Ziemniak and M. Hanson, “Zinc treatment effects on corrosion behavior of 304 stainless steel in high temperature, hydrogenated water,” *Corros. Sci.*, vol. 48, no. 9, pp. 2525–2546, Sep. 2006, doi: 10.1016/J.CORSCI.2005.10.014.
[29] A. G. Crouch and J. Robertson, “Creep and oxygen diffusion in magnetite,” *Acta Metall. Mater.*, vol. 38, no. 12, pp. 2567–2572, Dec. 1990, doi: 10.1016/0956-7151(90)90268-L.
[30] D. D. Macdonald, “Some Advantages and Pitfalls of Electrochemical Impedance Spectroscopy,” *CORROSION*, vol. 46, no. 3, pp. 229–242, Mar. 1990, doi: 10.5006/1.3585096.
[31] A. E. Bolzán and L. M. Gassa, “Comparative EIS study of the adsorption and electro-oxidation of thiourea and tetramethylthiourea on gold electrodes,” *J. Appl. Electrochem.*, vol. 44, no. 2, pp. 279–292, Feb. 2014, doi: 10.1007/s10800-013-0621-7.
[32] Y. C. Tang and A. J. Davenport, “Magnetic Field Effects on the Corrosion of Artificial Pit Electrodes and Pits in Thin Films,” *J. Electrochem. Soc.*, vol. 154, no. 7, p. C362, 2007, doi: 10.1149/1.2736662.
[33] L. Guo, E. Lovell, N. Wilson, P. Burdett, L. F. Cohen, and M. P. Ryan, “The electrochemical behaviour of magnetocaloric alloys La(Fe,Mn,Si)13Hx under magnetic field conditions,” *Chem. Commun.*, vol. 55, no. 25, pp. 3642–3645, 2019, doi: 10.1039/c9cc00640k.
[34] R. N. Clark, R. Burrows, R. Patel, S. Moore, K. R. Hallam, and P. E. J. Flewitt, “Nanometre to micrometre length-scale techniques for characterising environmentally-assisted cracking: An appraisal,” *Heliyon*, vol. 6, no. 3, p. e03448, 2020, doi: 10.1016/j.heliyon.2020.e03448.
[35] I. A. Maione, C. Zeile, L. V. Boccaccini, and A. Vaccaro, “Evaluation of EM loads distribution on DEMO blanket segments and their effect on mechanical integrity,” *Fusion Eng. Des.*, vol. 109–111, pp. 618–623, Nov. 2016, doi: 10.1016/j.fusengdes.2016.02.035.